Linear versus Self-Sustained Interdecadal Thermohaline Variability in a Coupled Box Model

ILYA RIVIN* AND ELI TZIPERMAN

Environmental Sciences, The Weizmann Institute of Science, Rehovot, Israel

(Manuscript received 30 May 1996, in final form 29 October 1996)

ABSTRACT

Recent studies of decadal/interdecadal climate variability suggested two main classes of mechanisms: self-sustained (supercritical) oscillations due to the internal nonlinearity of the ocean and linear (subcritical) thermohaline oscillations driven by stochastic atmospheric forcing. The authors use a coupled ocean–atmosphere meridional box model to carefully examine these two alternatives. It is shown that a weakly nonlinear relation between the north–south density gradient in the ocean and the meridional ocean transport can lead to self-sustained oscillations. A nonlinear relation between the SST and the air–sea heat flux can also lead to self-sustained oscillations, although indications are given that the air–sea heat flux depends linearly on the SST for a wide range of SST perturbations. It is thus concluded that, if interdecadal climate variability is due to self-sustained oscillations, the necessary nonlinearity must be related to internal ocean dynamics rather than to the air–sea interaction or to nonlinear atmospheric dynamics. The box model results are used to discuss a simple criterion, based on the probability distribution function of the meridional circulation time series, for differentiating between self-sustained and linear variability. This criterion could not rule out either the linear or nonlinear hypotheses for the thermohaline variability in the GFDL coupled general circulation model run of Delworth, Manabe, and Stouffer. This may indicate that the variability in the coupled general circulation model is near critical.

1. Introduction

Since the work of Bjerknes (1964) it is generally believed that the oceanic thermohaline circulation (THC) plays an important role in interdecadal climate variability. There is now a most interesting body of work on climate stability and variability that is based on a variety of ocean-only models from box models to ocean general circulation models (GCMs), mostly under mixed boundary conditions (Bryan 1986). These studies may be roughly divided into two groups differing in the energy source of the oscillations. In the first group, the THC variability was described as self-sustained oscillations due to internal nonlinearity of the ocean model (e.g., Welander 1982; Weaver et al. 1991; Winton and Sarachik 1993; Chen and Ghil 1995; Cai et al. 1995). In the case of self-sustained THC oscillations, the role of the atmospheric weather variability is only to randomize the oscillations resulting from the oceanic nonlinearity. In the second group of studies (e.g., Mikolajewicz and Maier-Reimer 1990; Bryan and Hansen 1995; Griffies and Tziperman 1995, hereafter GT95) thermohaline variability is mostly linear and is driven by external stochastic atmospheric forcing. The atmospheric noise is the source of energy for the variability in this second class, and no oceanic variability exists without this external stochastic forcing.

In order to try to eliminate artifacts due to the uncertain surface boundary conditions of ocean-only models (Zhang et al. 1993; Tziperman et al. 1994; Rahmstorf and Willebrand 1995; Power and Kleeman 1994), one can analyze THC variability in coupled ocean–atmosphere models (Delworth et al. 1993; hereafter D93) where the air–sea flux formulation is less arbitrary.

Assuming that the D93 3D coupled model THC variability reflects present day decadal climate variability somewhat more realistically than various ocean-only models under idealized boundary conditions, it is important to understand the energy source of the variability in this model. GT95 interpreted the D93 variability as a damped linear thermohaline oscillator, continuously excited by atmospheric noise. While GT95 were able to explain many of the features of the D93 THC oscillations, they could not completely exclude the possibility that the D93 oscillations were due to self-sustained variability, randomized by atmospheric noise. Moreover, Cai et al. (1995), Greatbatch and Peterson (1996), and Chen and Ghil (1995) suggested that the small am-

*Permanent affiliation: St. Petersburg Branch, P. P. Shirshov Institute of Oceanology, St. Petersburg, Russia.

Corresponding author address: Dr. Eli Tziperman, Environmental Sciences, The Weizmann Institute of Science, 76100 Rehovot, Israel. E-mail: citziper@weizmann.weizmann.ac.il

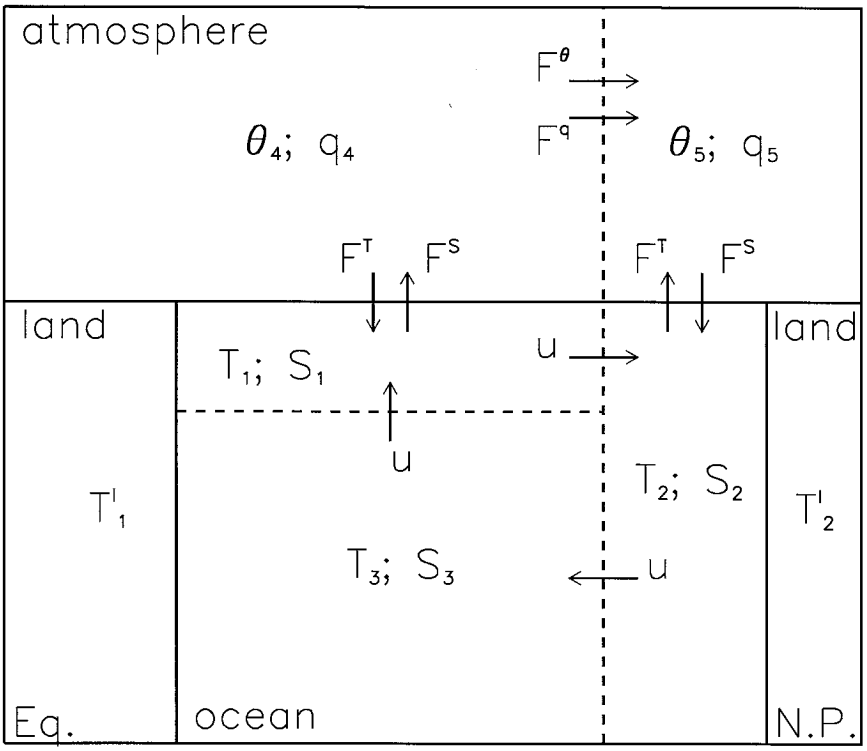

FIG. 1. The box model geometry.

plitude nonlinear self-sustained oscillatory regime generated in their ocean GCMs were similar to that described by D93.

The present work deals with the issue of linear variability versus self-sustained nonlinear variability. The main questions we address are: (i) What are the types of nonlinearities that may result in self-sustained interdecadal THC oscillations? (ii) Could a nonlinearity in the ocean–atmosphere interaction be responsible for self-sustained THC oscillations? (iii) How can one recognize whether THC oscillations are linear or nonlinear (self sustained) in the presence of noisy atmospheric forcing? These questions are dealt with in the context of 2D meridional models only, in the hope of illuminating the more complex behavior of 3D models as well.

For this purpose we use a simple coupled box model that enables us to thoroughly investigate some of the underlying physical mechanisms of climate variability, hopefully also relevant to more complicated models. The box model's parameterizations as well as the methodology and formulation of the coupling between the ocean and atmosphere submodels are motivated by those in coupled GCMs. The coupled box model is hemispheric, and includes three ocean boxes and two atmospheric boxes (Fig. 1). The ocean model has temperature and salinity as prognostic variables and uses a simple relation between the north–south density gradient and the ocean meridional transport. The atmospheric box model divides the atmosphere into two boxes, assumed well-mixed, one representing the midlatitudes and one the polar region. The atmospheric model includes prognostic equations for temperature and a diagnostic expression for the humidity in each box. The heat and moisture exchange between the atmospheric boxes depends on the temperature gradient between these boxes. The representation of radiation and the bulk formula used to calculate the air–sea fluxes are taken to be nonlinear, as in atmospheric GCMs. These nonlinear representations, more complex than used in various previous atmospheric box models (e.g., Birchfield 1989; Nakamura et al. 1994) are required in order for us to be able to examine, in section 4, the range in which the atmospheric response to SST perturbations is linear. The coupled model is described in full detail in the appendix. Similar coupled box models were used for different purposes by Kagan et al. (1984), Birchfield (1989), and Nakamura et al. (1994).

The D93 oscillations raise several additional interesting issues. One example is the view of these oscillations as being inherently thermohaline (D93, GT95) versus the view that salinity is not an important factor in these oscillations (Greatbatch and Peterson 1996). A second issue is the role of the horizontal circulation (D93; Greatbatch and Peterson 1996) versus the 2D meridional thermohaline mechanism of GT95. However, in the present study we ignore these issues and concentrate on the issue of nonlinear self-sustained oscillations versus damped oscillations driven by external noise. Our

model is a simple meridional model, and the oscillations we analyze are inherently thermohaline, but the analysis of linear versus nonlinear variability of this model should shed light on the same issue in different models as well. The value of a detailed analysis of simple meridional models has been demonstrated numerous times in the past, and we feel that such simple models are useful in the present context as well.

The outline of this paper is as follows: The mechanism of linear THC variability described by GT95 using an ocean-only box model is briefly demonstrated for our coupled ocean–atmosphere box model in section 2. In section 3 we examine various unexplored nonlinearities of the ocean–atmosphere system that can lead to self-sustained THC variability. This includes a nonlinear relation between the oceanic meridional transport and the meridional density gradient, and a nonlinear relation between the SST and air–sea heat fluxes. Section 4 discusses the dependence of air–sea fluxes on the SST, using an uncoupled atmospheric box model. Since this response appears to be linear over a wide range of parameters, we conclude that nonlinear THC oscillations are most likely to be a result of internal ocean nonlinearities. In section 5 we examine a way of distinguishing between linear oscillations driven by stochastic forcing and nonlinear oscillations randomized by noise. Our analysis raises the interesting possibility that the D93 GFDL coupled model oscillations are near critical, that is, on the border between the self-sustained and linear regimes. Our conclusions are presented in section 6.

2. Linear thermohaline oscillations in a coupled box model

Tziperman et al. (1994) considered the linear stability analysis of a 4-box meridional model of the thermohaline circulation under mixed boundary conditions (fixed evaporation minus precipitation, $[E - P]$, and a restoring condition for the temperature). When the model was in a thermally dominant regime, with sinking at high latitudes and upwelling in midlatitudes, the stability analysis revealed two possible oscillatory regimes under mixed boundary conditions, depending on the amplitude of the salinity forcing (i.e., the amplitude of the air–sea fresh water fluxes, $[E - P]$). A weak salinity forcing led to an oscillatory stable regime in which an initial perturbation to the steady-state solution results in exponentially decaying oscillations. A stronger salinity forcing led to an unstable steady-state solution for which an initial perturbation caused exponentially growing oscillations, eventually leading to another, stable, steady state. The strength of the salinity forcing (implied $[E - P]$ field) may be increased by running the model under restoring surface boundary conditions for the salinity, using a shorter salinity restoring time γ_s^{-1}, or a larger specified meridional salinity gradient $S_1^* - S_2^*$, before switching to mixed boundary conditions. Numerical experiments carried out by GT95 with a nonlinear ocean box model showed that a box model put in the damped oscillatory regime and forced with a moderate amplitude stochastic forcing displays only linear THC variability in spite of the nonlinear (quadratic) model equations. In this section we examine whether the replacement of the linear mixed boundary conditions by a nonlinear atmospheric box model could result in nonlinear self-sustained oscillatory behavior.

a. The thermohaline oscillation mechanism

Let us briefly describe the mechanism of THC oscillations presented in GT95 using an ocean-only box model under mixed boundary conditions. The same mechanism will be shown later to hold for the linear THC oscillations in our coupled box model as well as for the nonlinear THC oscillations discussed in section 3.

The main components of the oscillation mechanism proposed in GT95 are the positive salinity and negative temperature feedbacks, and the phase lag between the northern and southern boxes. Although we use a somewhat different box configuration here, the same mechanism applies to our model. Consider a steady-state solution of the ocean box model with ''sinking'' in the polar box so that the overturning circulation is positive, that is, from box 1 to box 2 (Fig. 1), and let us describe one complete cycle of the oscillation. Given a small positive initial transport perturbation u', this anomalous circulation advects the steady temperature and salinity gradients so that box 1 becomes fresher and colder and box 2 becomes saltier and warmer. The resulting salinity anomalies increase the north–south density gradient and therefore enhance the positive transport perturbation u'. The temperature anomalies, on the other hand, reduce the density gradient. Initially, the temperature anomalies are weaker because of the atmospheric restoring of SST anomalies. Eventually the north–south density gradient anomaly and the transport anomaly are weakened by the increasing temperature anomalies and by the advection of the anomalous salinity by the mean transports. The growing circulation anomaly therefore reaches a maximum value and starts decaying. The circulation anomaly approaches zero simultaneously with the density anomaly in the polar box, but because of the phase lag between the north and south surface boxes, there is still a cold and fresh anomaly in the surface midlatitude box. This fresh salinity anomaly is advected poleward and causes the salinity anomaly in the polar box to cross the zero point and become negative. The cycle described above now repeats, but with the temperature, transport, and salinity perturbations of opposite signs.

The two-box Stommel (1961) ocean model that is very similar to the one used here does not have an oscillatory behavior in the thermally dominant regime. One wonders if the oscillation arises here because of the dependence of the transport on the deep densities, a dependence that cannot occur in the Stommel model. To examine this, we froze the deep density in the ocean

TABLE 1. The model runs used in this study, the boundary conditions and initial conditions used, and the general regime for each run. Asterisks denote a regime in which the ocean model is switched to mixed boundary conditions. The model parameters that differ from the standard ones listed in the appendix and the figures in which each run appears are indicated.

Run	Model/boundary conditions	Initial conditions	Details	Regime	Figures
1	Ocean/restoring	—	Weak salinity forcing	Damped oscillatory*	—
2	Ocean/restoring	—	Strong salinity forcing, [$S^*_{1,2}$ = (36.9, 34.0) psu]	Oscillatory unstable*	—
3	Coupled	Run 1		Damped oscillatory	—
4	Coupled	Run 1	3.5% stochastic forcing	Stochastic linear oscillations	2, 9
5	Coupled	Run 2	Nonlinear transport equation	Self-sustained oscillations	4a, 4b
6	Ocean/mixed	Run 2	Nonlinear heat flux	Self-sustained oscillations	4a, 4c
7	Atmosphere	Run 1	±5 SST perturbations	—	5, 6, 7
8	Coupled	Run 2	Nonlinear transport equation, 2.5% stochastic forcing	Self-sustained stochastic oscillations	8

box model under mixed boundary conditions to its steady-state value. The density was frozen only for the purpose of the transport calculation, and the deep temperature and salinity were free to evolve as before. Damped oscillatory as well as unstable oscillatory regimes can still be obtained, very similar in form to those obtained when the transport depended on all three free ocean densities. Thus, the delay in advecting salinity perturbations through a third box is the additional factor allowing the oscillatory behavior that does not exist in the Stommel two-box model.

b. *Linear oscillations in a coupled ocean–atmosphere box model*

Our coupled box model contains many more nonlinearities than the ocean-only model, such as the quadratic meridional transport of heat and moisture in the atmosphere (A5), longwave radiation cooling of the atmosphere (A7), and the surface energy balance equation (A8). Could these additional nonlinearities produce nonlinear self-sustained THC oscillations? We find that when increasing the salinity forcing used to spin up the ocean-only box model before coupling it to the atmospheric model, the response of the thermohaline circulation in the coupled model is linear as in the ocean-only case described above. That is, a coupled model run initialized with relatively weak salinity forcing (run 1, Table 1) results in a damped oscillatory response with a period of 91 years and a decay time of 53 years. Initializing the coupled model with stronger salinity forcing (run 2) leads to exponentially growing oscillations and to a switch to a different steady state, and not to self-sustained oscillations. The mechanism of the oscillations is that described in detail by GT95 and briefly in section 2a. A related linear damped oscillatory response of a coupled box model was described in Birchfield (1989), where it could have been anticipated due to the linearized atmospheric submodel being used.

c. *Stochastically forced linear thermohaline oscillations*

In order to produce a continuous THC variability from the above damped oscillatory response, an external forcing is needed (GT95). We add a stochastic term to the meridional heat and moisture transports between the atmospheric boxes by setting the meridional transport coefficients in (A5) to

$$\tilde{K}^{\{\theta,q\}} = K^{\{\theta,q\}}(1 + N\psi). \tag{1}$$

Here ψ is a unit variance Gaussian Markov process with a correlation time of 1 week, and N is an adjustable noise amplitude set in our experiments to $N = 0.04$. This may be viewed as a parameterization of the atmospheric weather in the coupled box model. Note that the noise in (1) does not modify the global heat and moisture content of the atmospheric submodel but only their distribution between the atmospheric boxes. Figure 2a shows the behavior of the ocean transport within the coupled model, when put in a damped oscillatory regime (that is, initialized from run 1) and coupled to the noisy atmospheric model (1). In order to isolate the decadal variability from the high-frequency noise, a 10-yr low-pass filter was applied to the circulation time series (D93; GT95). The filtered and nonfiltered time series of the oceanic meridional circulation are shown in Fig. 2a. The atmospheric noise produces a high-frequency response and, in particular, excites irregular linear THC oscillations dominated by the damped oscillatory mode described by GT95.

Also shown in Fig. 2 are the temperature and salinity contributions to the ocean density anomalies in the polar ocean box, showing the slight phase delay between them that is characteristic of these thermohaline oscillations. The use of a coupled box model allows us to also examine the atmospheric response, which is shown in the same figure. The atmospheric temperature, and therefore also the air–sea fluxes, adjust quickly to the ocean temperature changes induced by THC variability. The atmospheric temperature (Fig. 2c) oscillates, therefore, almost in phase with the temperature of the correspond-

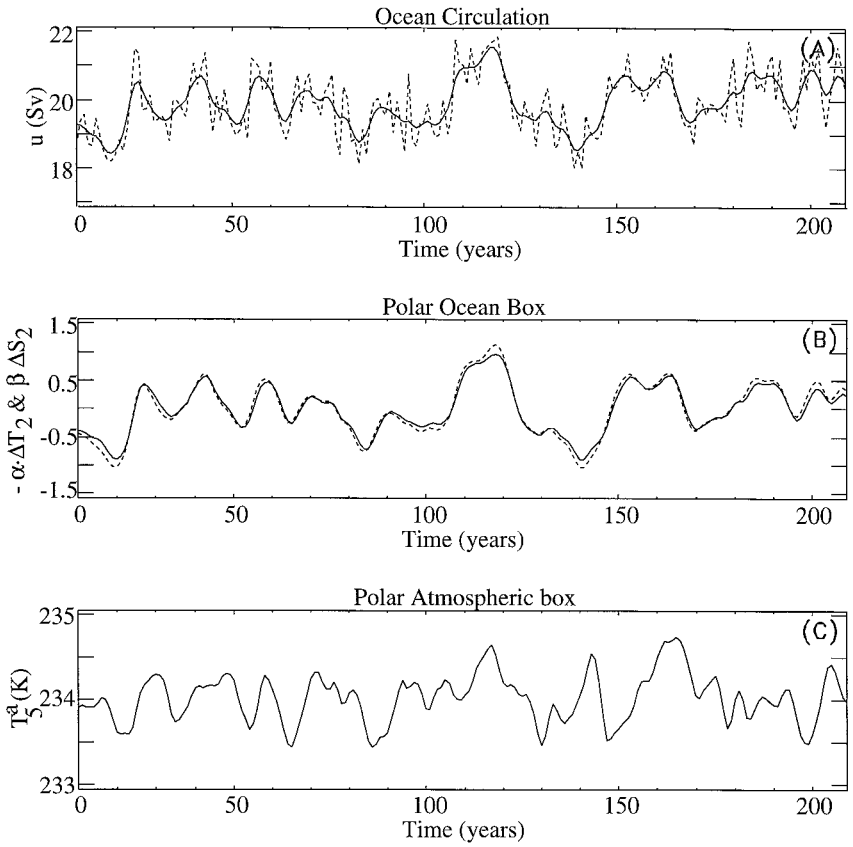

FIG. 2. Stable linear oscillations in the coupled model forced by noise in the atmospheric meridional transports (run 4, Table 1). (a) Ocean circulation anomaly time series without filtering (dashed line) and after low-pass filtering (solid line). (b) The contributions of temperature and salinity to the density in the polar ocean box. (c) Atmospheric temperature in the polar atmospheric box.

ing underlying ocean boxes, and so do the air–sea fluxes (not shown).

We conclude that while the atmospheric box model is highly nonlinear, simply coupling it to the ocean model does not necessarily lead to a regime with nonlinear self-sustained THC oscillations. This observation will be explained in section 4.

3. Nonlinear self-sustained thermohaline oscillations

For sufficiently nonlinear dynamics, self-sustained THC oscillations are possible and no external excitation is needed to produce THC variability. In fact, much of the recent literature about THC variability is about self-sustained variability in ocean GCMs. It is especially important, therefore, to use simplified models in order to isolate possible nonlinearities leading to such variability. Welander (1986) discussed two self-sustained thermohaline oscillators. One is due to a flip–flop local nonlinear convection mechanism (see also Welander 1982; Lenderink and Haarsma 1994; Rahmstorf 1994; Yin 1995). This mechanism is based on a response of the large-scale overturning circulation to the local vertical density profile at the sinking region. In contrast, the 2D nonlinear mechanism presented below relies on the global determination of the THC by the large-scale density gradients. We feel it is useful to examine these very different possibilities with the understanding that the real ocean may be expected to lie somewhere between these two extremes.

A second self-sustained oscillator discussed in Welander (1986) is a thermohaline Howard–Malkus oscillator, involving the nonlinear advection of temperature–salinity perturbations around the meridional thermohaline cell, and therefore characterized by a very long timescale (Winton and Sarachik 1993; Drijfhout et al. 1996).

Let us now discuss two specific nonlinearities that are quite different from the ones surveyed above and that may lead to self-sustained decadal climate variability. As throughout the paper, we concentrate on 2D meridional mechanisms.

a. Nonlinear relation between the THC and density gradient

Box models of the thermohaline circulation have normally followed Stommel (1961) in making the THC depend linearly on the large-scale density gradients. This has found some support in the calculations of Hughes and Weaver (1994), who showed such a linear relation in steady-state solutions of their ocean GCM. However, the possibility of a slight nonlinear dependence of the THC on the density gradients can clearly not be ruled out in general, especially not in the context of time-dependent situations. Let us therefore consider the possibility of such a nonlinearity (see also Cessi 1994).

We initialized our model from the results of an ocean-only run under strong salinity forcing (run 2, Table 1). If the linear ocean transport equation (A2) is used, coupling to the atmospheric model and introducing a small perturbation to the steady-state solution results in exponentially growing oscillations, eventually switching to another steady state.

The desired effect of nonlinearity would be to limit this exponential growth of the perturbation transport. Let us write the linear transport equation (A2) as $u = \bar{u} + u' = \bar{u} + u_0\Delta_n\rho'$, where the overbar denotes an ocean-only steady-state circulation value, prime denotes a perturbation from the steady state, and $\Delta_n\rho$ is the nondimensional north–south density gradient (A2). The desired nonlinearity may be obtained by making the coefficient u_0 a function of the density gradient, so that the anomalous transport u' is made less sensitive to the density gradient anomaly $\Delta_n\rho'$ for larger amplitudes of the density gradient anomaly. This motivates the following nonlinear relation between ocean transport and density gradient, shown in Fig. 3:

$$u = \bar{u} + u' = \bar{u} + \xi(u_0, \Delta_n\rho')\Delta_n\rho', \tag{2}$$

where

$$\xi(C,x) = \begin{cases} C\dfrac{x_+}{x}\left[k\left(\left[\dfrac{x}{x_+}\right]^{1/k} - 1\right) + 1\right] & \text{if } x > x_+ \\ C & \text{if } x_+ \geq x \geq x_- \\ C\dfrac{x_-}{x}\left[k\left(\left[\dfrac{x}{x_-}\right]^{1/k} - 1\right) + 1\right] & \text{if } x < x_-. \end{cases} \tag{3}$$

The product $u' = \xi(C, \Delta_n\rho') \times \Delta_n\rho'$ is continuous in $\Delta_n\rho'$, has a continuous first derivative, and is monotonically increasing (Fig. 3). We use $C \equiv u_0 = 7$Sv (Sv $\equiv 10^6$ m^3 s^{-1}), $x_+ \equiv \Delta_n\rho'_+ = 0.5 \times 10^{-5}$, $x_- \equiv \Delta_n\rho'_- = -0.5 \times 10^{-5}$, $k = 3$.

Using the nonlinear transport equation (2) in our coupled box model, and initializing the ocean model from a strong salinity forcing ocean-only run (run 2, Table 1), results in the self-sustained THC oscillations shown by the solid line in Fig. 4a. Given a small initial perturbation to the steady-state solution ($\bar{u} = 17.9$ Sv), the density anomaly is still within the linear portion of the transport equation ($\xi = $ const) so that the perturbation oscillates and initially grows exponentially. When the anomaly density gradient becomes large enough (so that $|\Delta_n\rho| > |\Delta_n\rho_\pm|$), the coefficient ξ becomes a nonlinear function of the density gradient. The further the model solution deviates from the steady-state value, the smaller this coefficient becomes. As a result, the amplitude saturates and the growing oscillations reach a limit cycle (Fig. 4b). The oscillation mechanism is the one described in section 2a.

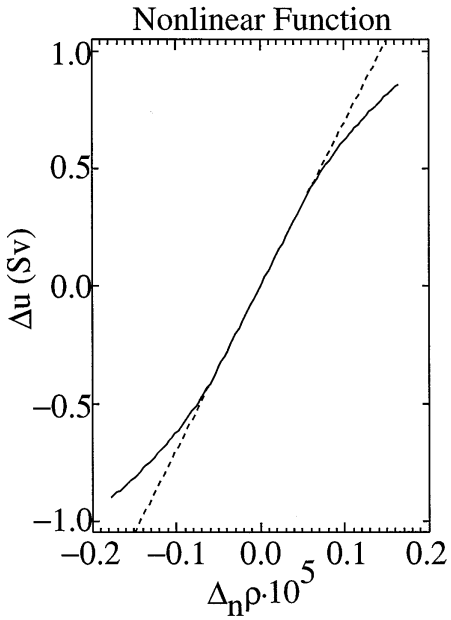

FIG. 3. The nonlinear relation between the meridional oceanic transport and the density gradient: $\xi(C, \Delta_n\rho')\Delta_n\rho'$ (solid line). The dashed line corresponds to the linear transport relation.

As seen in Fig. 3, the nonlinearity required to get self-sustained thermohaline oscillations is rather small. This is an important observation for evaluating the relevance of such nonlinearities to ocean GCMs.

b. Nonlinear dependence of the air–sea heat flux on SST

The commonly used restoring boundary conditions (Haney 1971) for the temperature in ocean-only models (A3) assume that the restoring atmospheric temperature T^* remains constant when the SST changes. This assumption implies one of two possible hypotheses: The first is of an infinite heat capacity of the atmosphere, resulting in no atmospheric temperature change as the atmosphere is absorbing the extra heat from the SST perturbation. The second possible hypothesis is that the atmosphere efficiently transports the anomalous mixed layer heat content due to the SST perturbation away from the SST perturbation area and then radiates it to

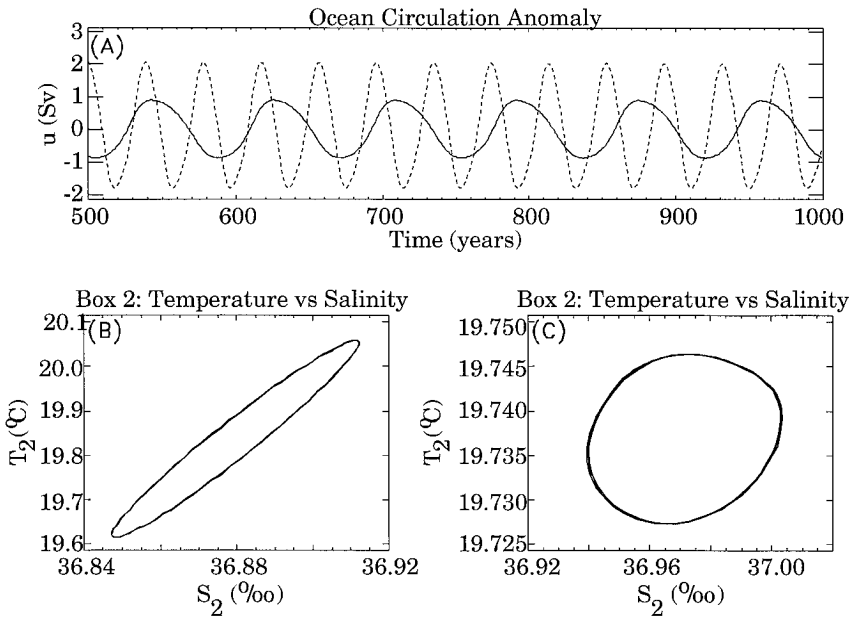

FIG. 4. Self-sustained thermohaline oscillations. (a) Ocean circulation anomaly. Solid line corresponds to the coupled model with nonlinearity in the ocean transport (run 5) and the dashed line corresponds to the air–sea heat flux nonlinearity in the ocean-only model (run 6). (b) Phase plane plot of T vs S for the northern ocean box for run 5. (c) Same as in b for run 6.

outer space (Bretherton 1982; Nakamura et al. 1994), leaving the local atmospheric temperature unchanged. These are obviously not realistic assumptions (Zhang et al. 1993), and, in fact, the temperature of the lower atmosphere quickly adjusts to SST changes according to the nonlinear atmospheric dynamics. The difference $T^* - \text{SST}$ may therefore, in principle, be a nonlinear function of the SST perturbation.

To examine the consequences of such a nonlinearity, consider the following simple nonlinear relation between the SST and air–sea heat flux, similar to the nonlinear transport equation in section 3a. In this air–sea heat flux parameterization, the air–sea heat flux is less sensitive to the SST for larger SST perturbations:

$$F'_{1,2} = \overline{F_{1,2}} + \xi(\gamma_T^e, T'_{1,2})T'_{1,2}, \tag{4}$$

where $C_{1,2} \equiv \gamma_T^e = 13.0V_{1,2} \times 10^{-8}\ \text{s}^{-1}$, $x_+ = 0.3°\text{C}$, $x_- = -1.1°\text{C}$, $k = 3$, and ξ is defined in (3).

Initializing the ocean-only box model from the steady state of the run under restoring boundary conditions with a strong salinity forcing (run 2, Table 1) and using the nonlinear air–sea heat flux relation (4) with fixed freshwater forcing, we obtain self-sustained thermohaline oscillations, shown in Figs. 4a (dash line) and 4c. The period of oscillations in the ocean-only model differs from that in the coupled model with the nonlinear transport equation (solid line in Fig. 4a), even though both nonlinear oscillations are based on the same linearly unstable oscillatory thermohaline mode. This is because the period of oscillation is set both by the linear oscillatory thermohaline mode discussed above and by the nonlinearity, through the values of $x_\pm$ in (3). The oscillation mechanism is again the one described for the linear oscillatory mode in section 2a. The next section uses a nonlinear atmospheric box model to examine the relevance of the above nonlinear dependence of the air–sea heat fluxes on the SST. We find that the air–sea flux anomalies are, in fact, linear with the SST perturbation amplitude. The relevance of the above results is therefore not in representing a realistic atmospheric nonlinearity, but in demonstrating how an unstable oscillatory ocean mode may saturate into a limit cycle by many different types of nonlinearity, two of which we examined in the sections 3a and 3b. Thus, it is demonstrated that the oscillation mechanism is separate from the nonlinearity, which may turn such an oscillation into a self-sustained limit cycle.

4. Dependence of air–sea fluxes on the SST

In section 3b we showed that if the SST and air–sea heat fluxes are nonlinearly related, our ocean box model supports self-sustained THC variability. However, we did not find such self-sustained oscillations when the ocean box model was coupled to the nonlinear atmospheric model (section 2b), indicating perhaps that the dependence of the air–sea heat flux on SST in the coupled box model may, in fact, be linear.

The atmospheric adjustment time is of the order of several months, while we are interested here in climate variability with timescales of a few decades. This means that the atmosphere has plenty of time to fully adjust

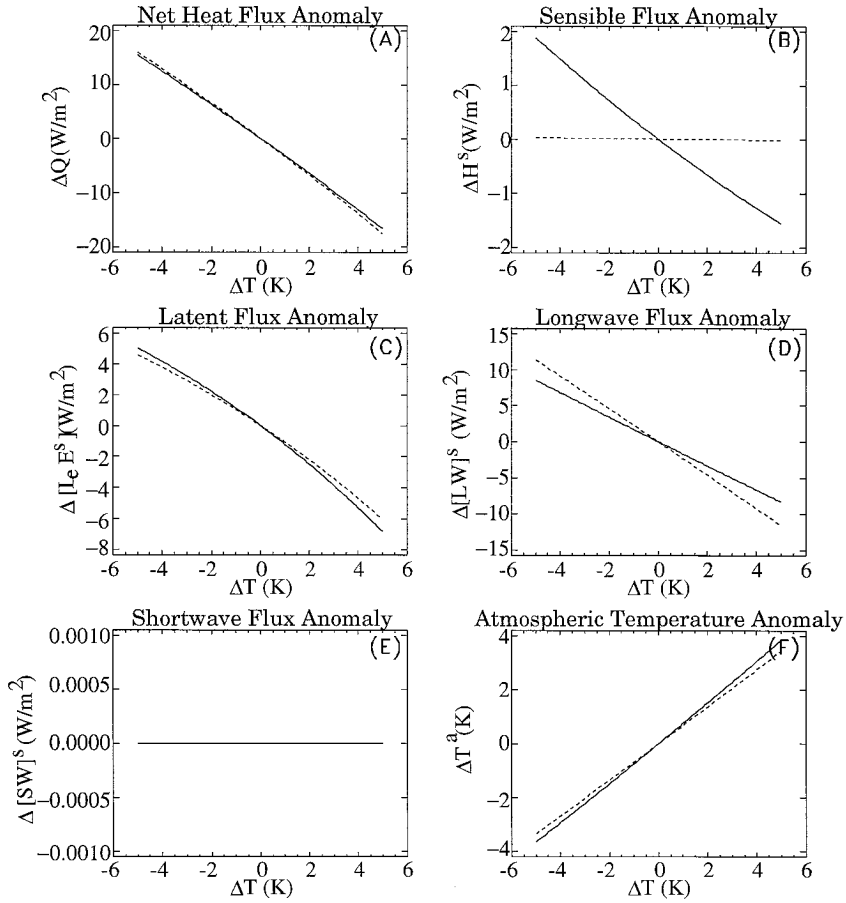

FIG. 5. Local response of the air–sea heat fluxes to SST perturbations in the uncoupled atmospheric submodel. Solid lines correspond to the flux anomaly in the polar atmospheric box 5 as a function of the SST perturbation in the same box. Dashed lines correspond to the flux anomaly in the midlatitude atmospheric box 4 as a function of the SST perturbation in the same box. (a) Net air–sea heat flux. (b) Sensible heat flux. (c) Latent heat flux. (d) Longwave radiative flux. (e) Shortwave radiative flux. (f) Atmospheric temperature perturbation due to the perturbation in SST.

to SST changes due to the oceanic variability. Our interest in the air–sea fluxes response to SST changes on interdecadal timescales implies, therefore, that we need to examine the steady-state atmospheric response to such SST changes, rather than the short-term (weeks to months) atmospheric adjustment toward this steady state.

We have therefore run a series of experiments in which we have perturbed the SST prescribed in each of our two-box atmospheric models, calculated the steady-state atmospheric response, and plotted the steady-state heat flux as function of the SST perturbation. The range of SST perturbations was ± 5°C, which is greater than the observed present-day decadal SST variability. One may assume that for very small SST perturbations the atmospheric response is expected to be linear. But precisely how large these SST perturbations may be before the linearity assumption breaks down is not clear and is the subject of this brief section (see also Rivin and Tziperman 1997).

Figure 5 portrays the behavior of the air–sea heat fluxes and their components as function of the SST perturbation amplitude. The interval between different SST perturbations is 0.1°C. The solid lines correspond to changes in the air–sea heat fluxes in the polar atmospheric box 5 as a response to SST changes in that same box, while dashed lines correspond to the air–sea heat flux changes in the midlatitude atmospheric box 4 due to changes in the box 4 SST. The results clearly show that both the net air–sea heat flux and its various components respond almost linearly to the SST changes. Let us consider each heat flux component and explain its linearity.

Sensible heat flux depends, according to (A11), only on the difference between the near-surface atmospheric temperature [T^* in (A11)] and the SST (T^s). Now, the

atmospheric temperature representing the 500-mb level responds linearly to SST perturbations (Fig. 5e), and the temperature T^* is linearly interpolated in pressure coordinates between the atmospheric and ocean temperatures (A13). Thus, the difference ($T^* - \text{SST}$) varies linearly with the SST, and the sensible heat flux may also be expected to be a linear function of the SST.

Consider next the longwave air–sea heat flux (A10), which is proportional to the difference between the fourth powers of the near-surface temperature and the SST. Let T' be the SST perturbation and $T^{a\prime}$ be corresponding atmospheric temperature anomaly. Then

$$\begin{aligned}[\text{LW}]^o &= \sigma_r[\nu^{\downarrow}(\overline{T^a} + T^{a\prime})^4 - (\overline{T} + T')^4] \\ &= \overline{[\text{LW}]^o} + \sigma_r[4(\nu^{\downarrow}(\overline{T^a}^3 T^{a\prime} - \overline{T}^3 T') \\ &\quad + 6(\nu^{\downarrow}(\overline{T^a}^2 T^{a\prime 2} - \overline{T}^2 T'^2) + O(T^{a\prime 3}, T'^3)].\end{aligned}$$

The ratio of the coefficients of the linear and quadratic terms in T' is proportional to the mean SST (T). Since these values are of the order of 10^2 (measured in kelvin), the quadratic term is negligible, and the longwave flux should react linearly to the SST perturbation.

The latent air–sea heat flux is calculated using (A12). Expanding the exponents in this expression in a Taylor series, it can again be shown that the latent flux in our model should also respond linearly to SST perturbations of the order of $\pm 5°$.

It is clear that the response of the air–sea heat flux should be linear for very small SST perturbations (Bretherton 1982). Our study indicates, in addition, that at least for our box model, the air–sea flux is a linear function of the SST for a wide range of SST perturbations. It is conceivable that the mechanisms that may make the air–sea fluxes depend on the SST in a nonlinear way may be missing in our box model, and our conclusions need, of course, to be confirmed by more complete models. Rivin and Tziperman (1997) demonstrated that the response of the air–sea heat flux in the NCAR Climate Community Model 1 (CCM1) atmospheric general circulation model to a number of SST perturbations is linear within a range of $\pm 3°$C. Their analysis suggests that the linearity of the air–sea flux response to SST perturbations may be a more robust finding than may be implied from the simple atmospheric box model used here (see also Power et al. 1995).

As the SST increases in a given box, the air temperature in this box increases, although less than the SST (Fig. 5f). As a result, the air–sea heat flux into the ocean decreases (Figs. 5a–d). The air temperature in the box with unperturbed SST also increases due to the changes in the atmospheric meridional heat flux, while the SST in this box remains constant in the atmosphere-only box model. Therefore, the air–sea heat fluxes in this box increase (Figs. 6a–d). Hence, the signs of the air–sea heat flux anomalies in the boxes with perturbed and unperturbed SST are opposite. The sensitivity of the air–sea heat flux is smaller in the box with the unperturbed SST because changes in the air temperature there are much smaller (Figs. 5f and 6f).

The response of the air–sea freshwater flux calculated by the atmospheric box model to SST perturbations is examined in Fig. 7. The response is very nearly linear. As seen in the figure, the sensitivity of the air–sea freshwater flux is very weak in this box model. The linearity of the $E - P$, however, is also found in the AGCM study of Rivin and Tziperman (1997), where the sensitivity is significantly larger. As already indicated by Marotzke (1994) and Capotondi and Saravanan (1996), the underlying assumption of the mixed boundary conditions that the freshwater flux does not depend on the ocean state is inaccurate.

The main point to bear in mind from the above analysis concerning self-sustained THC variability is that no tendency toward saturation is found in the air–sea flux response to large SST perturbations, as opposed to the parameterization considered in section 3b. This conclusion was confirmed in the atmospheric GCM study of Rivin and Tziperman (1997). Thus, ocean nonlinearities such as those considered in section 3 are the most likely source of self-sustained thermohaline variability in addition, of course, to 3D mechanisms not considered here.

5. Distinguishing between linear and nonlinear THC variability in the presence of noise

The last section leads to the conclusion that nonlinear self-sustained THC oscillations, if they exist in nature, must be related to oceanic nonlinearities, excluding nonlinearity in the air–sea fluxes. But can present-day THC variability be described as self-sustained or is it linear and driven by atmospheric noise? Clearly, the approach in answering this question would have to be different from that of the last section, as our simple model cannot examine and rule out all possible ocean nonlinearities. We thus try to develop a simple criterion to distinguish between self-sustained oscillations randomized by noise (e.g., Cai et al. 1995; Chen and Ghil 1995) and linear oscillations forced by external stochastic forcing (GT95). We then apply this criterion to the D93 coupled model THC variability in the hope that understanding the variability in this coupled model will contribute to the understanding of the actual climate system variability.

To develop and demonstrate this criterion we first apply it to the output of our box model. We generated two time series of the ocean meridional circulation using our coupled ocean–atmosphere box model. The first time series is from a coupled box model run using the strong salinity initialization and the nonlinear ocean transport equation (2), with an additional stochastic noise added to the atmospheric meridional fluxes (Fig. 8, run 8, Table 1). Note that this run is characterized by self-sustained thermohaline variability even without the stochastic forcing, and the noise serves only to ran-

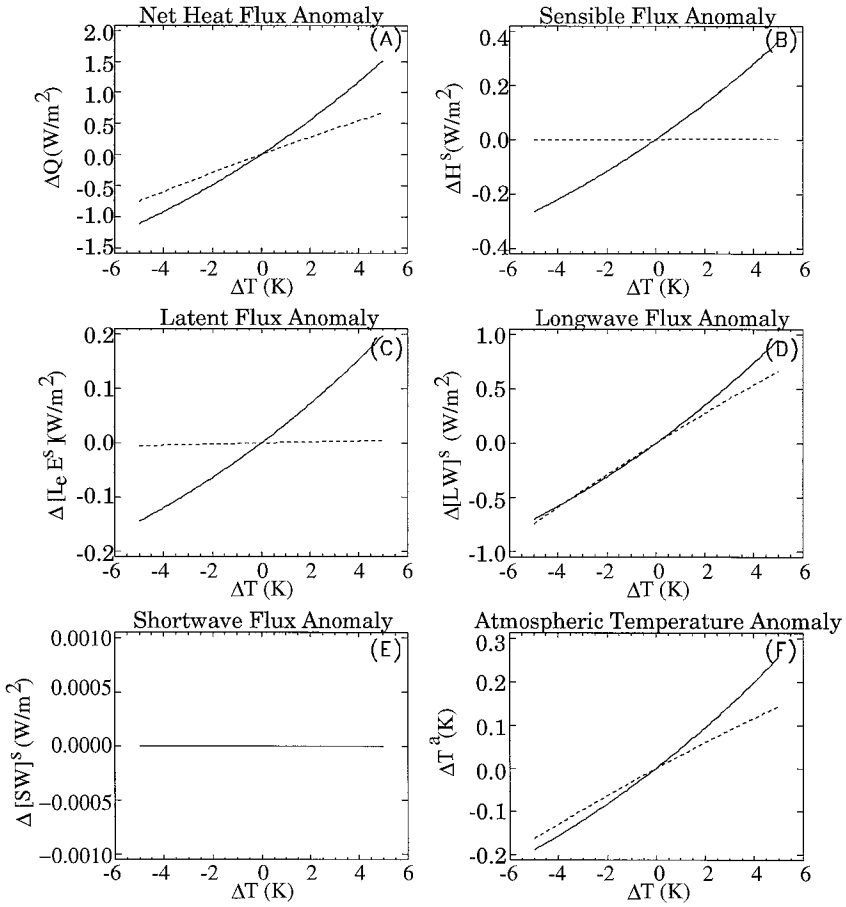

FIG. 6. The remote response of air–sea heat fluxes to SST perturbations in the uncoupled atmospheric submodel. The solid lines show the air–sea flux anomaly in the polar atmospheric box 5 as a function of the SST perturbations in the midlatitude box. The dashed lines show the flux anomaly in the midlatitude atmospheric box 4 as a function of the SST perturbation in the polar box.

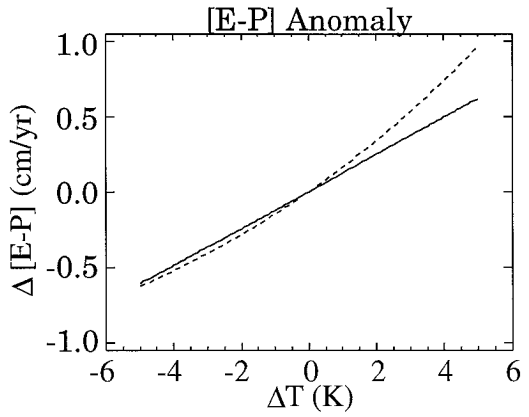

FIG. 7. Freshwater air–sea flux anomaly as function of the local SST perturbation, for the midlatitude atmospheric box 4 (solid line) and for the polar atmospheric box 5 (dashed line).

domize the THC variability. The second time series is from the stochastically driven linear variability of run 4 (Fig. 9).

Figure 8a shows a 200-yr fragment of the filtered time series from the nonlinear variability of run 8. The power spectrum of the nonfiltered time series (Fig. 8b) has a peak at the dominant frequency of the self-sustained oscillations, about 90 years. The autocorrelation of the filtered time series is shown in Fig. 8c. The autocorrelation indicates the existence of oscillations and decays for large lag times due to the randomizing effect of the added atmospheric noise. A temperature versus salinity phase plane plot for box 2 is shown in Fig. 8d, demonstrating the same thermohaline mechanism as for the linear plot described in GT95 (compare to their Fig. 5b).

A useful diagnostic that can often be used to differentiate between linear and nonlinear oscillations is the probability distribution function (pdf) of the time series. The pdf is calculated as a histogram giving the number of occurrences of a given amplitude in the time series,

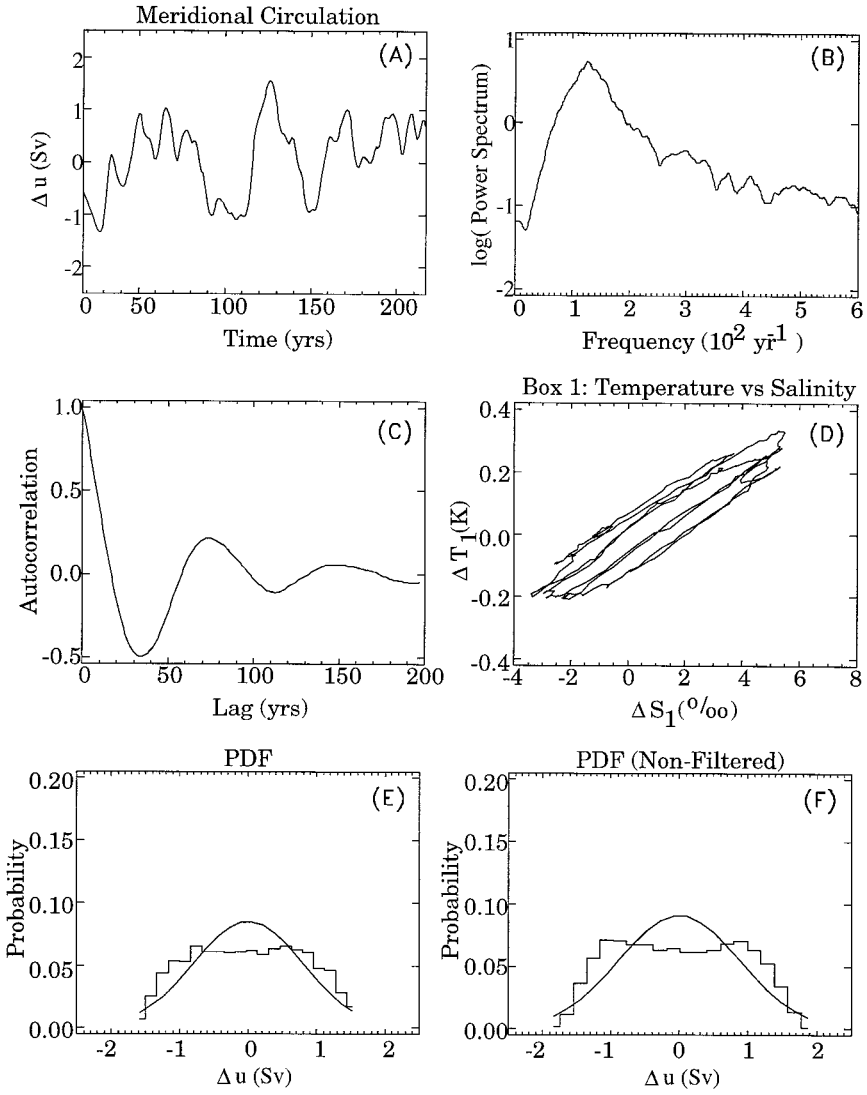

FIG. 8. Nonlinear self-sustained THC oscillations in the coupled model, with 2.5% noise in the atmospheric meridional fluxes of heat and moisture (run 8). (a) Ten-year low-pass filtered time series of the meridional oceanic circulation. (b) Fourier power spectrum of the nonfiltered meridional circulation time series. (c) Autocorrelation function for the filtered meridional circulation time series. (d) *T–S* phase plane plot for the upper midlatitude box using filtered time series. (e) Probability distribution function for the filtered meridional circulation time series. (f) As in (e) but for the nonfiltered time series.

normalized by the total number of occurrences. If the stochastic forcing is Gaussian, linear oscillations should be characterized by a Gaussian pdf, while nonlinear oscillations often deviate significantly from a Gaussian form. Figure 8e shows the pdf calculated from the low-pass filtered time series of nonlinear variability (run 8), and the pdf for the corresponding nonfiltered time series is shown in Fig. 8f. The pdf shapes in both cases are non-Gaussian and are characterized by a double peak, characteristic of nonlinear oscillations. This happens because in self-sustained oscillations that resemble a simple sin(*t*) function, one is more likely to find the solution near the extremes of the functions than near its mean value. The pdf is somewhat affected by the 10-yr filtering and the pdf for the filtered time series has a slightly less pronounced double-peak structure. However, the non-Gaussian nature of the pdf is clear and was found to be quite a robust feature for reasonably small-amplitude noise. A χ^2 test for the pdf of the nonfiltered time series gives a probability of more than 99.9% that the pdf for the nonlinear run is non-Gaussian. We also find that, as the noise level increases, the pdf becomes more Gaussian-like, even for a coupled model run which displays self-sustained variability in the absence of atmospheric noise.

The above self-sustained oscillatory solution random-

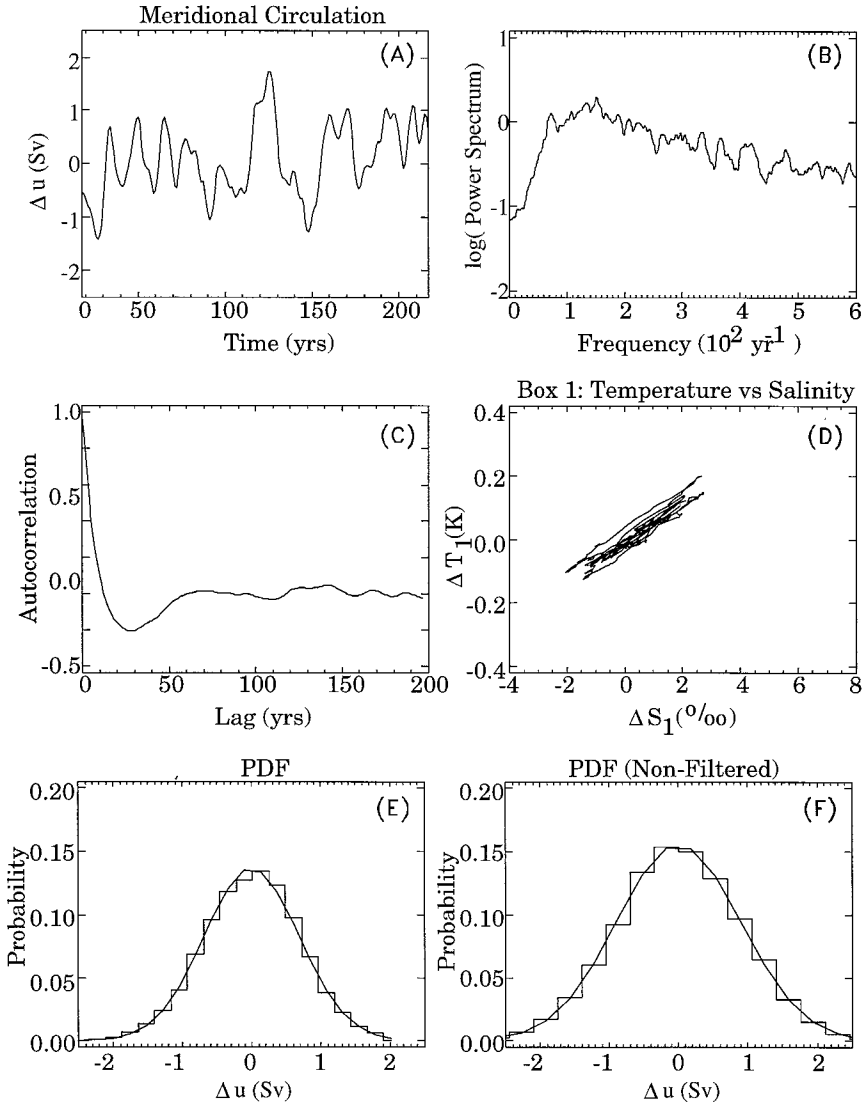

FIG. 9. As in Fig. 8 but for the damped linear thermohaline oscillations in the coupled box model excited by 3.5% noise in the atmospheric meridional transports (run 4).

ized by noise is now compared to a time series from a model run (run 4) under a linear damped oscillatory regime forced with 3.5% stochastic forcing (Fig. 9). As can be seen by comparing Figs. 8a–d to Figs. 9a–d, the rms variability, autocorrelation function, power spectrum, and phase plot behaviors are quite similar for both runs (more precisely, we made them similar by tuning the model), making it difficult to differentiate the linear and nonlinear oscillations. However, the pdf in the linear case is close to Gaussian for both filtered and nonfiltered time series. The χ^2 test gives a probability of 78% that the pdf in the linear case is Gaussian for the nonfiltered time series, while for the filtered time series the test is somewhat less significant. This provides a possible criterion for differentiating linear from nonlinear behavior. Note that the mechanism of nonlinearity does not matter: it could be the nonlinear transport mechanism used here, the 3D gyre effect found in Cai et al. (1995), or any other.

We now turn our attention to the overturning time series from the coupled model of D93. After removing the linear trend in the time series (as was also done by D93 and GT95), the analyses of Figs. 8 and 9 were repeated for this time series. Figure 10 shows the time series, Fourier spectrum, autocorrelation function, and probability distribution function for the North Atlantic's overturning index in the coupled GCM of D93. While the time series probability distribution function is not completely Gaussian (the χ^2 probability that the pdf is Gaussian is 64%), the shape of the probability distribution function for both filtered and nonfiltered time series seems near-Gaussian (Figs. 10d and 10e). How-

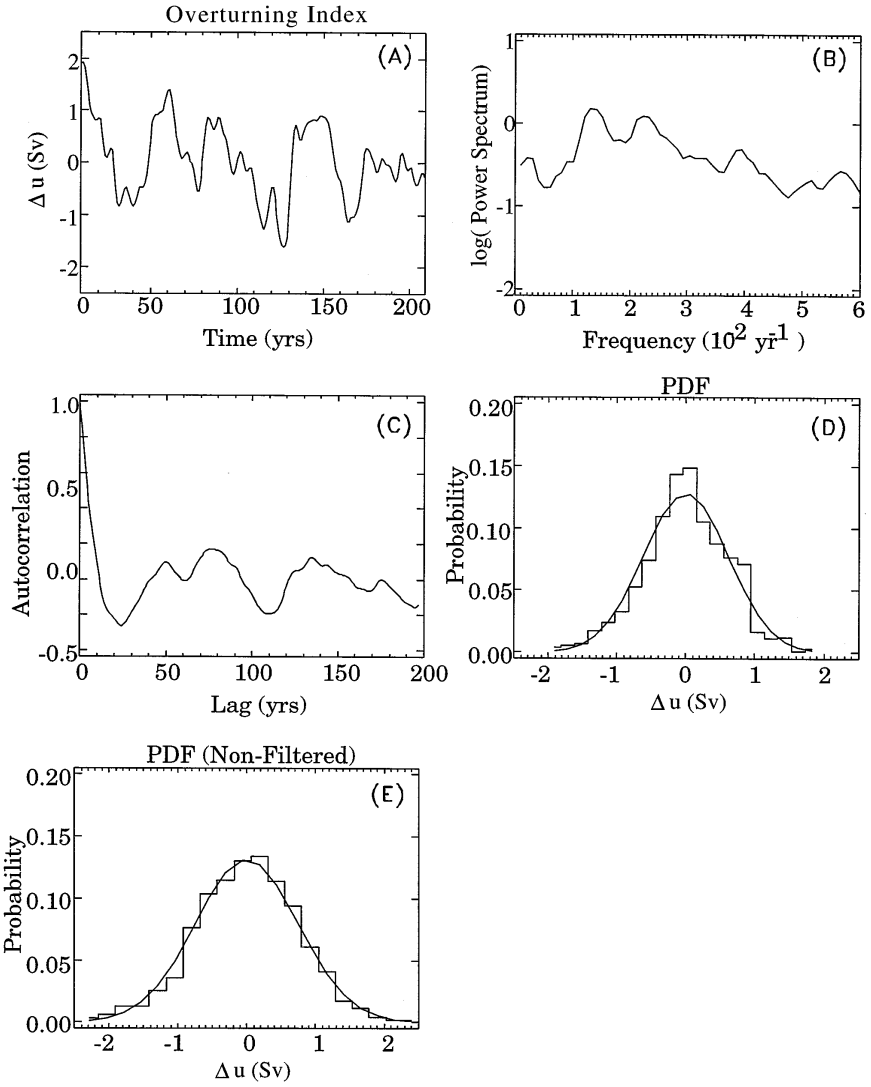

FIG. 10. Overturning index in the coupled GCM run of D93. (a) Time series of filtered time series. (b) Fourier power spectrum of nonfiltered time series. (c) Autocorrelation function of filtered time series. (d) Probability distribution for the filtered time series. (e) Probability distribution for the nonfiltered time series.

ever, the statistical significance is insufficient to rule out neither the Gaussian nor the non-Gaussian hypotheses. This seems to indicate that, if the oscillations in D93 are self-sustained, the nonlinearity is not very dominant over the atmospheric stochastic forcing. The analysis of the pdf may suggest that both nonlinearity and stochastic forcing are important. These oscillations may be termed ''near critical'' in the sense that, if they are nonlinear and self-sustained, they are only weakly so, indicating that the coupled general circulation model is close to the bifurcation point leading from damped linear oscillations (GT95) to self-sustained oscillations (Cai et al. 1995). We conclude by noting that the length of the time series is rather limited due to the cost of running such coupled models. Future studies with longer coupled model time series may be able to further examine the issue of nonlinearity using the approach discussed here.

6. Conclusions

The main objective of this study was to critically examine two possible classes of interdecadal thermohaline variability mechanisms, namely, linear oscillations excited by stochastic atmospheric forcing and nonlinear self-sustained oscillations. We have shown that a nonlinear thermohaline oscillation arises from the combination of two factors: a linearly unstable thermohaline oscillation mechanism and a nonlinearity that limits the growth of the unstable oscillations and leads to a limit-cycle behavior. The linear thermohaline oscillation

mechanism, such as that of Griffies and Tziperman (1995), can result, under strong salinity forcing, in exponentially growing oscillations and may lead to a switch to a different steady state. An appropriate nonlinearity, such as the nonlinear relation between meridional density gradient and the oceanic circulation, can limit the growth of the linearly unstable oscillations and lead to a limit cycle and self-sustained thermohaline oscillations. We emphasize that the oscillation mechanism may be independent of the nonlinearity in the model, as it was in our simple coupled box model. We have thus shown how self-sustained 2D thermohaline oscillations arise from a bifurcation that makes the basic state oscillatory unstable. It would be interesting to see if self-sustained oscillations that are inherently 3D, as seen in numerous 3D ocean general circulation models (e.g., the recent example of Drijfhout et al. 1996), can also be explained as a combination of a linearly unstable oscillation and a nonlinear growth-limiting mechanism.

We have considered two possible nonlinearities leading to self-sustained thermohaline oscillations in our box model. The first and possibly more relevant one was a slightly nonlinear relation between the large-scale meridional density gradients and the oceanic meridional overturning. The second such nonlinearity was a nonlinear relation between the air–sea fluxes and the SST. We argue, however, based on both our box model and the GCM study of Rivin and Tziperman (1997), that the air–sea heat flux response to SST anomalies may be linear in a wide range of SST perturbation amplitudes. Thus, the coupling of an ocean model to a nonlinear atmospheric model could not lead, by itself, to self-sustained thermohaline variability. We conclude that, if self-sustained thermohaline variability occurs in nature, it is most likely the result of internal oceanic nonlinearity.

The mechanism of self-sustained thermohaline variability considered here, is, in a sense, the opposite of the Welander (1982) flip–flop convection mechanism that may also result in self-sustained oscillations (Welander 1982, 1986; Lenderink and Haarsma 1994; Rahmstorf 1994; Yin 1995). In the flip–flop mechanism, the large-scale overturning circulation is controlled by the local vertical density gradient at the small sinking area. In the alternative mechanism considered here (GT95), on the other hand, the thermohaline variability is controlled by the large-scale horizontal density gradients. The actual oceanic behavior is expected to be somewhere between these two extremes, with both the local vertical density profile at the sinking area and the large-scale horizontal density gradients determining the overturning circulation.

We approached the problem of distinguishing linear thermohaline oscillations, driven by stochastic atmospheric forcing, from self-sustained thermohaline variability in which the atmospheric noise only serves to randomize the oscillations. Using our coupled box model, we showed that the two classes may be qualitatively differentiated using the probability distribution function for the overturning time series. An application of this criterion to the coupled GCM overturning time series of Delworth et al. (1993), however, could not rule out linear nor nonlinear behavior. Longer coupled-model time series may enable a better determination of the role of nonlinearity versus noise. We speculate that the inability to determine the role of nonlinearity may be because the coupled GCM is near the bifurcation point leading from damped linear thermohaline oscillations to self-sustained oscillations. In this case, of course, one may expect higher-resolution models in which nonlinearity plays a more dominant role to be characterized by self-sustained thermohaline variability (McWilliams 1996). The emphasis on the analysis of model behavior in the above discussion clearly indicates that there is insufficient data to examine the role of nonlinearity in the variability of the actual North Atlantic thermohaline circulation with a satisfactory degree of confidence.

Acknowledgments. We thank two anonymous reviewers for their constructive comments. We are grateful to Tom Delworth for providing us the results of D93. This work is partly supported by the Israeli Science Foundation. Partial funding for IR is also provided by a fellowship from the Feinberg Graduate School, The Weizmann Institute of Science.

APPENDIX

Description of the Coupled Ocean–Atmosphere Box Model

Our coupled box model contains both oceanic and atmospheric components. The land area is represented, and the ice cover is fixed to constant representative values.

a. Ocean box model

The ocean box model is a three-box hemispheric version of Joyce's (1991) model (Fig. 1); the same representation of the ocean was used in the coupled box model of Nakamura et al. (1994). The ocean is represented by three boxes: surface (first) and deep (second) midlatitude boxes and a polar (third) box; all of the boxes are assumed well mixed. The governing equations are

$$\dot{T}_i = V_i^{-1}|u|(T_j - T_i) + F_i^T,$$
$$\dot{S}_i = V_i^{-1}|u|(S_j - S_i) + F_i^S, \qquad i = 1, 2, 3, \quad \text{(A1)}$$

where u is the transport between boxes and

$$u = u_0\Delta_n\rho,$$
$$\Delta_n\rho = -\alpha T_2 + \beta S_2 - \delta(-\alpha T_1 + \beta S_1) - (1 - \delta)(-\alpha T_3 + \beta S_3), \quad \text{(A2)}$$

$$j = \begin{cases} (3, 1, 2) \text{ for } i = (1, 2, 3) & \text{if } u > 0 \\ (2, 3, 1) \text{ for } i = (1, 2, 3) & \text{if } u \le 0, \end{cases}$$

$$F_3^T \equiv 0, \qquad F_3^S \equiv 0, \qquad \delta \equiv \frac{D_1}{D_1 + D_3}.$$

Here T_i, S_i, V_i, and D_i are the temperature, salinity, volume, and depth of the ith box correspondingly. Note that the above linear relation between the transport and the nondimensional north–south density gradient $\Delta_n\rho$ is replaced by the nonlinear relation (2) for runs 5 and 8 (Table 1). The air–sea heat and implied freshwater fluxes are given by $F_{1,2}^T$ and $F_{1,2}^S$.

In the ocean-only model runs, the surface heat flux is calculated by restoring the temperature of boxes 1 and 2 to the reference temperatures $T_{1,2}^*$:

$$F_{1,2}^T = \gamma_T(T_{1,2}^* - T_{1,2}), \tag{A3}$$

where γ_T is the restoring coefficient (inverse restoring time) for temperature. In restoring boundary conditions (runs 1 and 2, Table 1) the salinity forcing is $F_{1,2}^S = \gamma_S(S_{1,2}^* - S_{1,2})$, with γ_S the restoring coefficient for the salinity and $S_{1,2}^*$ the restoring salinities for the surface boxes. In mixed boundary conditions (run 6) $F_{1,2}^S$ are fixed. In the coupled box model runs, the heat and freshwater forcing are calculated in the atmospheric submodel. The implied salt flux F_i^S is calculated by multiplying the freshwater flux by a reference salinity $S_0 = 35$ psu.

The standard ocean model parameters are $u_0 = 5.7$ Sv, $\alpha = -1468 \times 10^{-7}$ K^{-1}, $\beta = 7.61 \times 10^{-4}$ psu^{-1}, $V_{1,2,3} = (267, 12, 801) \times 10^5$ km^3, $D_{1,2,3} = (1, 4, 3)$ km, $T_{1,2}^* = (20.2, -7.0)$°C, $S_{1,2}^* = (36.8, 34.3)$ psu, $\gamma_{T_{1,2}} = 3.17V_{1,2} \times 10^{-8}$ s^{-1}, $\gamma_{S_{1,2}} = 6.17V_{1,2} \times 10^{-8}$ s^{-1}.

b. Atmospheric box model

The atmospheric box model is based on that of Kagan et al. (1984). The atmosphere is divided into two boxes: midlatitude (fourth) and polar (fifth) (Fig. 1).

The heat and moisture equations for the ith box are

$$\left.\begin{aligned} \frac{\partial\theta_i}{\partial t} &= F_i^\theta + \frac{2^\xi g}{p_i^s c_p}(H_i^s + H_i^r) + Q_i^p \\ 0 &= F_i^q + \frac{g}{p_i^s}(E_i - P_i) \end{aligned}\right\}, \quad i = 4, 5, \tag{A4}$$

where θ_i is the potential temperature of the ith box; q_i is the specific humidity, $\xi = R/c_p$, $R = 287$ J kg^{-1} K^{-1} is the gas constant for dry air; $c_p = 1004$ J kg^{-1} K^{-1} is the atmospheric specific heat at constant pressure; $g = 9.8$ m s^{-2} is the acceleration due to gravity; p_i^s is the surface pressure; F_i^θ and F_i^q are the meridional transports of heat and moisture, Q_i^p is the heating due to the condensation; H_i^s and H_i^r are the rates of heating from the lower boundary and due to interior radiation effects, and E_i is the evaporation and P_i precipitation.

Assuming that the meridional heat and moisture transports in the atmosphere are carried by the synoptic-scale motions only, we can use Stone's (1972) parameterization

$$\begin{pmatrix} F_i^\theta \\ F_i^q \end{pmatrix} = (-1)^i \frac{a_i}{a_4 + a_5} \begin{pmatrix} K^\theta(\theta_4 - \theta_5) \\ K^q(q_4 - q_5) \end{pmatrix} |\theta_4 - \theta_5|, \quad i = 4, 5; \tag{A5}$$

where a_i are the areas of the ith box and K^θ, K^q and are proportionality constants for the meridional heat and moisture fluxes.

Specific humidity is evaluated by specifying the mean atmospheric relative humidity r^a in each box. The specific humidity is then calculated using $q_i = r_i^a q_m(T_i^a, p^a)$ (Saltzman 1979), where the saturation specific humidity q_m is a known function of pressure and temperature,

$$q_m(T, p) = 380.96p^{-1}\, 10^{7.63 - 1848.5/(T - 31.0)}. \tag{A6}$$

The radiation flux is divided into longwave and shortwave (ultraviolet and visible) radiation fluxes; that is, $H^r = [\text{LW}] + [\text{SW}]$. Following Saltzman (1968),

$$\left.\begin{aligned} [\text{LW}]_i &= \sigma_r[P_i^{\text{LW}}(T_i^s)^4 - (\nu_i^\uparrow + \nu_i^\downarrow)(T_i^a)^4] \\ [\text{SW}]_i &= P_i^{\text{SW}}(1 - A_i^a)S_i^{t\downarrow} \end{aligned}\right\}, \quad i = 4, 5; \tag{A7}$$

where $\sigma_r = 5.6701 \times 10^{-8}$ W m^{-2} K^{-4} is the Stefan–Boltzmann constant; P_i^{LW} and P_i^{SW} are the absorption coefficients for longwave and shortwave radiation in the ith box; $\nu_i^\uparrow$ and $\nu_i^\downarrow$ are the upward and downward emissivity of longwave radiation in the ith box; A_i^a is the atmospheric albedo in the ith box; $S_i^{t\downarrow} = S_\odot \overline{\cos h_{\odot}}_i$ is the shortwave radiation at the top of the atmosphere in the ith box; $S_\odot = 1370$ W m^{-2} is the solar constant; and $\overline{\cos h_{\odot}}_i$ is the annual mean cosine of the solar zenith angle averaged over ith box. Here θ_i is the weight-averaged potential temperature of the ith box. Assuming that it represents the potential temperature at the mean level $p^a = 500$ mb, we can calculate the temperature of the ith box as $T_i^a = \theta_i/2^\xi$. The surface temperature $T_i^s = f_j T_j^r + (1 - f_j)T_j$, where j is the index of the underlying land/ocean box under the ith atmospheric box, T_j^r is the land (or sea ice) temperature, and f_j is the relative area of land and sea ice specified in the ith atmospheric box.

Continental surface temperature and sea ice temperature, as well as heat flux into the ocean, are all calculated as explained below from the heat budget equation,

$$[\text{SW}]_i^s + [\text{LW}]_i^s + H_i^s + L_e E_i^s = Q_i, \quad i = 4, 5; \tag{A8}$$

where superscript s denotes variables at the surface (sea, land, or ice), and $L_e = 2.501 \times 10^6$ J kg^{-1} is the latent heat of evaporation. For the radiative fluxes we use the expressions suggested by Saltzman (1968), and the turbulent fluxes of heat and moisture at the surface are calculated by the well-known bulk formulas

$$[\mathrm{SW}]_i^s = (1 - P_i^{\mathrm{SW}})(1 - A_i^a)(1 - A_i^s)S_i^{t\downarrow} \quad \text{(A9)}$$

$$[\mathrm{LW}]_i^s = \sigma_r[\nu_i^{\downarrow}(T_i^a)^4 - (T_i^s)^4] \quad \text{(A10)}$$

$$H_i^s = -C_i^s c_p(T_i^* - T_i^s) \quad \text{(A11)}$$

$$E_i^s = -C_i^s(r_i^* q_m(T_i^*, p_i^*) - r_i^s q_m(T_i^s, p_i^s)) \quad \text{for } i = 4, 5; \quad \text{(A12)}$$

where A^s is the surface albedo, $C_i^s = C_D(RT_i^s/p_i^s)v_i^*$, C_D is the drag coefficient; superscript * denotes variables at the near-surface atmospheric level p^* (chosen $p_i^* = 0.9985p_i^s$, which correspond to a height of about 12 m); v_i^* is the frictional wind velocity; and r_i^s is the prescribed relative humidity. To evaluate T_i^* we use the same interpolation formula as Saltzman (1979):

$$T_i^* = \sigma^{\xi}[2^{\xi+1}(1 - \sigma)T_i^a - (1 - 2\sigma)T_i^s], \qquad i = 4, 5; \quad \text{(A13)}$$

where $\sigma = p_i^*/p_i^s$.

Over land and ice, one requires no net flux into the surface, sets $Q_i \equiv 0$, and uses (A8)–(A13) to calculate the land (ice) temperature T^{ℓ} by an iteration process. The parameters used are $C_D = C_D^{\ell}$, $T_i^s = T_i^{\ell}$, $A_i^s = A_i^{\ell}$ for $T_i^{\ell} > 0$°C and $A_i^s = A_i^i$ for $T^{\ell} \le 0$°C, $r_i^s = r_i^{\ell}$ $r_i^* = r_i^{*\ell}$. The superscripts ℓ and i denote variables over the land and ice correspondingly.

Over the ocean, the flux into the lower boundary in the atmospheric box model is the air–sea flux: $Q_i \equiv F_{i-3}^T \neq 0$. One then specifies the SST (T^o) or obtains it from the ocean model and uses (A8)–(A13) to calculate the air–sea heat flux F_i^T. The parameters used are $C_D = C_D^o$, $T_i^s \equiv T_{i-3}$, $A_i^s = A_i^o$, $r_i^s = r_i^o$, $r_i^* = r_i^{*o}$.

Precipitation P_i is calculated as a reminder term in the second expression of (A4) after substituting (A5) and (A12). Heating due to condensation is $Q_i^p = L_e P_i/c_p$.

The standard atmospheric model parameters are $a_{5,6} = (534, 16) \times 10^5$ km^2, $f_{5,6} = (30, 30)$%, $p_{5,6}^s = (1013, 1013)$ mb, $v_{5,6}^* = (0.3, 0.3)$ m s^{-1}, $K^{\theta} = 1.16 \times 10^{12}$ K^{-1} s^{-1}, $K^q = 0.58$ K^{-1} s^{-1}, $r_{5,6}^{*o} = (90, 100)$%, $r_{5,6}^{*\ell} = (50, 40)$%, $r_{5,6}^{\ell} = (60, 40)$%, $r_{5,6}^o = (100, 100)$%, $P_{5,6}^{\mathrm{LW}} = (95, 95)$%, $P_{5,6}^{\mathrm{SW}} = (26, 43)$%, $\nu_{5,6}^{\uparrow} = (0.80, 0.82)$, $\nu_{5,6}^{\downarrow} = (1.30, 1.28)$, $A_{5,6}^a = (30, 38)$%, $A_{5,6}^o = (6, 11)$%, $A_{5,6}^{\ell} = (22, 40)$%, $A_{5,6}^i = (70, 70)$%, $C_{D5,6}^{\ell} = (5, 5) \times 10^{-2}$, $C_{D5,6}^o = (1.4, 1.4) \times 10^{-2}$.

c. Method of coupling

The ocean and atmosphere submodels are coupled in a similar way to that used in coupled GCMs. First, the uncoupled ocean submodel is run to a steady-state under restoring boundary conditions for both temperature and salinity. Then, the steady-state temperatures of the upper midlatitude and polar ocean boxes are used as a lower boundary condition to run the atmosphere-only model to a steady state. The differences between the restoring fluxes in the ocean-only steady state and the air–sea heat and $[E - P]$ fluxes obtained in the atmosphere-only model run are saved to be used as flux correction terms for the ocean model in the coupled model run. In the coupled model run, both models are initialized from their uncoupled spinup solutions and are run synchronously, exchanging data each day. Heat and freshwater fluxes are sent from the atmospheric model to the ocean, and SST is sent from the ocean to the atmosphere. The flux correction terms are added to the air–sea fluxes in order to prevent a drift of the coupled model from the uncoupled steady states due to systematic errors in both submodels [see Manabe et al. (1991) and Sausen et al. (1988) for further discussion of this ''flux adjustment'' or ''flux correction'' method].

A brief summary of model runs, including the model parameters that differ from the standard ones listed above, and the figure numbers in which each run appears, are given in Table 1.

REFERENCES

Birchfield, G. E., 1989: A coupled ocean–atmosphere climate model: Temperature versus salinity effects on the thermohaline circulation. *Climate Dyn.,* **4,** 57–71.

Bjerknes, J., 1964: Atlantic air–sea interaction. *Advances in Geophysics*, Vol. 10, Academic Press, 1–82.

Bretherton, F. P., 1982: Ocean climate modeling. *Progress in Oceanography*, Vol. 11, Pergamon Press, 93–129.

Bryan, F., 1986: High-latitude salinity effects and interhemispheric thermohaline circulation. *Nature,* **323,** 301–304.

Bryan, K., and F. C. Hansen, 1995: A stochastic model of North Atlantic climate variability in a decade to century time-scale. *Proc. Workshop on Decade-to-Century Time Scales of Climate Variability*, Irvine, CA, Natl. Res. Counc., Board of Atmos. Sci. and Climate, Natl. Acad. Sci., 363–364.

Cai, W., R. J. Greatbatch, and S. Zhang, 1995: Interdecadal variability in an ocean model driven by a small, zonal redistribution of the surface buoyancy flux. *J. Phys. Oceanogr.,* **25,** 1998–2010.

Capotondi, A., and R. Saravanan, 1996: Sensitivity of the thermohaline circulation to surface buoyancy forcing in a two-dimensional ocean model. *J. Phys. Oceanogr.,* **26,** 1039–1058.

Cessi, P., 1994: A simple box model of stochastically forced thermohaline flow. *J. Phys. Oceanogr.,* **24,** 1911–1920.

Chen, F., and M. Ghil, 1995: Interdecadal variability of the thermohaline circulation and high-latitude surface fluxes. *J. Phys. Oceanogr.,* **25,** 2547–2568.

Delworth, T., S. Manabe, and R. J. Stouffer, 1993: Interdecadal variations of the thermohaline circulation in a coupled ocean–atmosphere model. *J. Climate,* **6,** 1993–2011.

Drijfhout, S., C. Heinze, M. Latif, and E. Maier-Reimer, 1996: Mean circulation and internal variability in an ocean primitive equations model. *J. Phys. Oceanogr.,* **26,** 559–580.

Greatbatch, R. J., and K. A. Peterson, 1996: Interdecadal variability and oceanic thermohaline adjustment. *J. Geophys. Res.,* **101,** 20 467–20 482.

Griffies, S. M., and E. Tziperman, 1995: A linear thermohaline oscillator driven by stochastic atmospheric forcing. *J. Climate,* **8,** 2440–2453.

Haney, R. L., 1971: Surface thermal boundary conditions for the ocean model. *J. Phys. Oceanogr.,* **1,** 241–248.

Hughes, T. M. C., and A. J. Weaver, 1994: Multiple equilibria of an asymmetric two-basin ocean model. *J. Phys. Oceanogr.,* **24,** 619–637.

Joyce, T. M., 1991: Thermohaline catastrophe in a simple four-box model of the ocean climate. *J. Geophys. Res.,* **96,** 20 393–20 402.

Kagan, B. A., V. A. Ryabchenko, and A. S. Safray, 1984: Simulation

of the seasonal evolution of the thermal regime of the ocean–atmosphere system. *Izv. Atmos. Oceanic Phys.*, **20,** 34–40.

Lenderink, G., and R. J. Haarsma, 1994: Variability and multiple equilibria of the thermohaline circulation associated with deep-water formation. *J. Phys. Oceanogr.*, **24,** 1480–1493.

Manabe, S., R. J. Stouffer, M. J. Spelman, and K. Bryan, 1991: Transient responses of a coupled ocean–atmosphere model to graduate changes of atmospheric CO_2. Part I: Annual mean response. *J. Climate,* **4,** 785–818.

Marotzke, J., 1994: Ocean models in climate problems. *Ocean Processes in Climate Dynamics: Global and Mediterranean Examples*, P. Malanotte-Rizzoli and A. R. Robinson, Eds., Kluwer Academic, 79–109.

McWilliams, J. C., 1996: Modeling the oceanic general circulation. *Annu. Rev. Fluid Mech.,* **28,** 215–248.

Mikolajewicz, U., and E. Maier-Reimer, 1990: Internal secular variability in an ocean general circulation model. *Climate Dyn.,* **4,** 145–156.

Nakamura, M., P. H. Stone, and J. Marotzke, 1994: Destabilization of the thermohaline circulation by atmospheric eddy transport. *J. Climate,* **7,** 1870–1882.

Power, S. B., and R. Kleeman, 1994: Surface heat flux parameterization and the response of ocean general circulation models to high-latitude freshening. *Tellus,* **46,** 86–95.

——, ——, R. Colman, and B. McAvaney, 1995: Modeling the surface heat flux response to long-lived SST anomalies in the North Atlantic. *J. Climate,* **8,** 2161–2180.

Rahmstorf, S., 1994: Rapid climate transitions in a coupled ocean–atmosphere model. *Nature,* **372,** 82–85.

——, and J. Willebrand, 1995: The role of temperature feedback in stabilizing the thermohaline circulation. *J. Phys. Oceanogr.*, **25,** 787–805.

Rivin, I., and E. Tziperman, 1997: Sensitivity of air–sea fluxes to SST perturbations. *J. Climate,* in press.

Saltzman, B., 1968: Steady state solution for axially-symmetric climatic variables. *Pure Appl. Geophys.*, **69,** 237–259.

——, 1979: Equilibrium climatic zonation deduced from a statistical-dynamical model. Rep. of the JOC Study Conf. on Climate Models, Vol. 2, GARP Publ. 22, 1049 pp. [Available from Secretariat, World Meteorological Organization, Case postale No. 5, CH-1211 Geneva 20, Switzerland.]

Sausen, R., K. Barthel, and K. Hasselmann, 1988: Coupled ocean–atmosphere models with flux correction. *Climate Dyn.,* **2,** 145–163.

Stommel, H., 1961: Thermohaline convection with two stable regimes of flow. *Tellus,* **13,** 224–230.

Stone, P. H., 1972: A simplified radiative–dynamical model for the static stability of rotating atmosphere. *J. Atmos. Sci.,* **29,** 405–418.

Tziperman, E., R. Toggweiler, Y. Feliks, and K. Bryan, 1994: Instability of the thermohaline circulation with boundary conditions: Is it really a problem for realistic models? *J. Phys. Oceanogr.*, **24,** 217–232.

Weaver, A. J., E. S. Sarachik, and J. Marotzke, 1991: Freshwater flux forcing of decadal and interdecadal oceanic variability. *Nature,* **353,** 836–838.

Welander, P., 1982: A simple heat-salt oscillator. *Dyn. Atmos. Oceans,* **6,** 233–242.

——, 1986: Thermohaline effects in the ocean circulation and related simple models. *Large Scale Transport Processes in Oceans and Atmosphere*, J. Willebrand and D. L. T. Anderson, Eds., NATO ASI Series, Vol. C190, D. Reidel, 163–200.

Winton, M., and E. S. Sarachik, 1993: Thermohaline oscillations induced by strong salinity forcing of ocean general circulation models. *J. Phys. Oceanogr.,* **23,** 1389–1410.

Yin, F. L., 1995: A mechanistic model of ocean interdecadal thermohaline oscillations. *J. Phys. Oceanogr.*, **25,** 3239–3246.

Zhang, S., R. J. Greatbatch, and C. A. Lin, 1993: A reexamination of the polar halocline catastrophe and implications for coupled ocean–atmosphere modeling. *J. Phys. Oceanogr.*, **23,** 287–299.